

## CN 2-1 and CS 5-4 observations toward Arp 299 with the SMA

JUNZHI WANG,<sup>1</sup> CHUNHUA QI,<sup>2</sup> SHANGHUO LI,<sup>3</sup> AND JINGWEN WU<sup>4,5</sup>

<sup>1</sup>*School of Physical Science and Technology, Guangxi University, Nanning 530004, People's Republic of China; junzhiwang@gxu.edu.cn*

<sup>2</sup>*Harvard-Smithsonian Center for Astrophysics, 60 Garden Street, Cambridge, MA 02138*

<sup>3</sup>*Korea Astronomy and Space Science Institute, 776 Daedeokdae-ro, Yuseong-gu, Daejeon 34055, Republic Of Korea*

<sup>4</sup>*University of Chinese Academy of Sciences, Beijing 100049, People's Republic of China*

<sup>5</sup>*National Astronomical Observatories, Chinese Academy of Sciences, Beijing 100101, People's Republic of China*

### ABSTRACT

Dense gas is the key for understanding star formation in galaxies. We present high resolution ( $\sim 3''$ ) observations of CN 2-1 and CS 5-4 as dense gas tracers toward Arp 299, a mid stage major merger of galaxies, with the Submillimeter Array (SMA). The spatial distribution of CN 2-1 and CS 5-4 are generally consistent with each other, as well as HCN 1-0 in literature. However, different line ratios of CS 5-4 and CN 2-1 are found in A, B, and C regions, with highest value in B. Dense gas fraction decreases from IC 694 (A), to NGC 3690 (B) and the overlap starburst region (C and C'), which indicates that circum-nuclear upcoming starburst in A and B will be more efficient than that in the overlap region of Arp 299.

*Keywords:* Galaxies: merger; Galaxies: individual: Arp 299

### 1. INTRODUCTION

Galaxy-galaxy interactions and merging play an important role in the formation and evolution of galaxies, and can trigger intense starburst activity and/or supply the fuel for AGN (Toomre & Toomre 1972; Springel et al. 2005). Studying molecular gas in merging galaxies is important for understanding merging process, triggering of nuclear and off-nuclear starbursts, and the process of star formation in extreme environments. Imaged with good spatial resolution, nearby major mergers allow detailed investigation of the exact location of molecular gas that directly fuels the star formation and/or nuclear activity.

Because of low upper-level energy and low critical density ( $\sim 5 \times 10^2 \text{cm}^{-3}$ ), low- $J$  (2-1, 1-0) transitions of CO lines are not necessarily good tracer of star-forming gas (Gao & Solomon 2004; Lada et al. 2012), which is better traced by lines of high-dipole moment molecules, such as HCN, HNC, HCO<sup>+</sup> and CS (Gao & Solomon 2004; Scoville et al. 2015; Imanishi et al. 2019; Li et al. 2021), or high  $J$  CO (Yao et al. 2003; Sakamoto et al. 2008; Mao et al. 2010). HCN 1-0 had been used to measure dense gas in a sample of galaxies to study the relation between star formation rate and dense gas mass (Gao & Solomon 2004). High resolution observations of HCN lines had been done toward several local major mergers, including Arp 299 (IC694+NGC3690) (Aalto et al. 1997; Casoli et al. 1999; Imanishi & Nakanishi 2006), Arp 220 (Scoville et al. 2015), NGC 6240 (Scoville et al. 2015), VV 114 (Saito et al. 2018), NGC 3256 (Harada et al. 2018), and NGC 4038 & NGC 4039 (the Antennae galaxy) (Bemis & Wilson 2019).

However, it was questioned whether HCN was an ideal tracer of dense gas in star forming regions of LIRGs/ULIRGs as HCN can be excited by the mid-IR pumping or shocks (Papadopoulos 2007), which can enhance HCN emission. On the other hand, HCN can be transferred to HNC and CN in molecular clouds under certain conditions. For example, it can be transferred to CN with the UV photons in PDRs, which can reduce the HCN flux despite the presence of dense molecular gas. Since multiple line observations of HCN 1-0, HCO<sup>+</sup> 1-0, HNC 1-0, and CS 3-2 toward a sample of more than 100 galaxies showed similar linear relationships between their luminosities and infrared luminosities, with a factor of several in variation of line ratios in different galaxies (Li et al. 2021), it is hard and not that important to do correction of conversion factor from HCN line luminosity to dense gas mass in individual galaxy. However, if we would like to probe the detailed dense gas distribution in galaxies, it is essential to observe other dense gas tracers, such as lines of CS, CN, HCO<sup>+</sup> and HNC, to obtain a better and unbiased view of the dense gas.

High resolution observations of dense gas tracers other than HCN lines had been done toward several nearby major mergers, including CS 7-6 in Arp 220 and NGC 6240 (Scoville et al. 2015), HCO<sup>+</sup> 1-0, 3-2, and 4-3, HNC 1-0, and CS 7-6 in VV 114 (Saito et al. 2018), HNC, HCO<sup>+</sup> and CS lines in NGC 3256 (Harada et al. 2018), and HCO<sup>+</sup> 1-0 and HNC 1-0 in the Antennae galaxy (Bemis & Wilson 2019). Due to different critical densities and possible different chemical abundances to that of HCN, the lines of other high dipole moment molecules showed different spatial distribution to that of HCN lines (Scoville et al. 2015; Saito et al. 2018; Harada et al. 2018; Bemis & Wilson 2019). Among those observed sources, Arp 220, NGC 6240 and NGC 3256 are late-stage mergers, while VV 114 is a mid-stage merger and the Antennae galaxy is at early-stage. Overlap starburst is found in the Antennae (Wang et al. 2004; Bemis & Wilson 2019), while nuclear starburst activities dominate star formation in these mid and late-stage mergers in VV 114, Arp 220, NGC 6240 and NGC 3256. Thus, Arp 299, as a mid-stage merger with both nuclear starburst and overlap region starburst (Alonso-Herrero et al. 2009), is an ideal source to study overlap starburst during merging process.

Arp299, at a distance of  $\sim 42$ Mpc (Casoli et al. 1999), had been observed at high resolution with <sup>12</sup>CO 1-0, <sup>13</sup>CO 1-0 and HCN 1-0 (Aalto et al. 1997; Casoli et al. 1999; Imanishi & Nakanishi 2006), HCO<sup>+</sup> 1-0 (Imanishi & Nakanishi 2006), <sup>12</sup>CO 3-2 and 2-1 (Sliwa et al. 2012), and CN 1-0 (Aalto 2004). HCN 1-0 showed not only different properties to that of CO 1-0 and 2-1, but also different to that of CN 1-0 (Aalto 2004) and HCO<sup>+</sup> 1-0 (Imanishi & Nakanishi 2006). Based on the high resolution data, most of HCN 1-0 emission comes from the left galaxy IC694 (Aalto et al. 1997; Casoli et al. 1999), while the strongest CN 1-0 emission, with similar critical density to that of HCN 1-0 (Shirley 2015), is at the overlap starburst region (Aalto 2004). It is necessary to use other dense gas tracers, such as CS lines, to better probe the dense molecular gas and determine the dense gas properties, including volume density, temperature, and chemistry in Arp 299.

In this paper, we will present high resolution observational results of CN 2-1 and CS 5-4 toward Arp 299 with the Submillimeter Array (SMA) (Ho et al. 2004). Observations and Data reduction will be described in §2, results and discussion will be present in §3, and a brief summary will be made in §4.

## 2. OBSERVATIONS AND DATA REDUCTION

The observations of CN 2-1 and CS 5-4 toward Arp 299 were taken with the SMA at compact configuration (Project ID: 2007B-S015, PI: Junzhi Wang) on March 19 th and 20 th, 2008, respectively. CN 2-1 line was set in the lower side band with the local oscillator (LO) frequency of 229.304 GHz, while CS 5-4 was in upper side band with LO frequency of 237.475 GHz. Callisto was used as flux calibrator, while the quasar J1924-292 was used as bandpass calibrator. Two quasars, J1153+495 and J0958+655, were used as gain calibrators to correct time dependent variations of both phase and amplitude. Standard calibrations for the uvdata were made with the IDL MIR package<sup>1</sup>, while imaging and deconvolution with nature weighting were made with CASA to obtain the final data cubes, after smoothing to the velocity resolution of 20 km s<sup>-1</sup> for both CN 2-1 and CS 5-4. The reference frequency used for data cube of CN 2-1 is 224.415 GHz, which is calculated from CN 2-1 ( $J=\frac{3}{2} - \frac{1}{2} F=\frac{5}{2} - \frac{3}{2}$ ) at rest frequency of 226.659543 GHz with  $z=0.01$ , and 242.510 GHz for CS 5-4 calculated from rest frequency of 244935.556 GHz with  $z=0.01$ . The beam sizes are  $3.12'' \times 2.98''$  with  $PA = -12.25^\circ$  for CN 2-1, and  $2.93'' \times 2.67''$  with  $PA = -36.95^\circ$  for CS 5-4, while the typical rms noise levels are about 10 mJy beam<sup>-1</sup> for both CN 2-1 and CS 5-4 at the velocity resolution of 20 km s<sup>-1</sup>. 1.3 mm continuum distribution is also obtained with line free channels of both CN 2-1 and CS 5-4 data, which provide a map with beam size of  $3.14'' \times 2.79''$ ,  $PA = -33.37^\circ$  and rms level of 0.65 mJy beam<sup>-1</sup>.

## 3. RESULTS AND DISCUSSION

As shown in Figure 1(a) and (b), 1.3 mm continuum emission in Arp 299 can be found in IC 694 (A), NGC 3690 (B) and overlap starburst region (C and C'). The coordinates of symbols '+', which indicate the locations of A, B, C and C', in Figure 1 and 2, are from 8.4 GHz continuum (Ramírez-Olivencia et al. 2022). The velocity integrated CN 2-1 emission is mainly from IC 694 (A) with peak emission at about 20 $\sigma$  level, while weak emission can also be seen near NGC 3690 (B) and the overlap starburst region (C and C') at 3 to 4 $\sigma$  level. CS 5-4 emission is also mainly from IC 694 (A) with peak emission at about 8 $\sigma$  level, while about 3 $\sigma$  signal is also detected near B region. The velocity integrated CN 2-1 and CS 5-4 overlaid on 1.3 mm continuum are presented in Figure 1(a) and (b), while spectra of CN 2-1 and CS 5-4 in A, B, and C regions are presented in Figure 1(c-e). A narrow CN 2-1 emission feature around

<sup>1</sup> <https://github.com/qi-molecules/sma-mir>

$C'$  region is found at the velocity around  $-100 \text{ km s}^{-1}$ . The velocity integrated map of this velocity component and the spectra of CN 2-1 and CS 5-4, are presented in Figure 2(a) and (b), respectively.

The spatial distributions of both CN 2-1 and CS 5-4 are generally consistent with that of HCN 1-0 (Aalto et al. 1997; Casoli et al. 1999; Imanishi & Nakanishi 2006) with strong emission in A and weak emissions in B and C( $C'$ ) regions, while the strong CN 1-0 emission in the overlap starburst regions of Arp 299 presented in Aalto (2004) seems not to be real signal. On the other hand, A and B+C regions had similar total CO 1-0 flux (Solomon et al. 1992), which were confirmed with high resolution observations (Aalto et al. 1997; Casoli et al. 1999). CO 2-1 showed similar spatial distribution to that of CO 1-0 (Sliwa et al. 2012). Single dish observations of HCO<sup>+</sup> and HCN 1-0 lines with IRAM 30meter telescope toward A and B+C regions also showed stronger emission in A than that of B+C regions with flux ratios between A and B+C regions of about 1.55 for HCO<sup>+</sup> 1-0 and 1.76 for HCN 1-0 (Jiang et al. 2011).

Amount of molecular gas in the overlap starburst regions (C and  $C'$ ) was further supported by high resolution observations of optically thin <sup>13</sup>CO 1-0 (Aalto et al. 1997; Casoli et al. 1999) and <sup>13</sup>CO 2-1 (Sliwa et al. 2012). The three main components (A, B, C+ $C'$ ) in Arp 299 have different gas properties. There are strong <sup>12</sup>CO emissions and amount of molecular gas traced by <sup>13</sup>CO 1-0 and 2-1, most of which are with high volume density traced by dense gas tracers in IC 694 (A), while only strong <sup>12</sup>CO, <sup>13</sup>CO and HCO<sup>+</sup> 1-0 emission without strong emission of tracers with critical density higher than that of HCN 1-0 were detected in the overlap starburst regions (C and  $C'$ ), which means that dense gas fraction is much less in C and  $C'$  than A. On the other hand, even though strong <sup>12</sup>CO 1-0 (Aalto et al. 1997; Casoli et al. 1999) and 2-1 (Casoli et al. 1999; Sliwa et al. 2012) were detected in NGC 3690 (B), the molecular gas is much less than that of IC 694 and the overlap starburst regions, based on <sup>13</sup>CO 1-0 (Aalto et al. 1997; Casoli et al. 1999) and <sup>13</sup>CO 2-1 (Sliwa et al. 2012) observations.

There are several hyperfine lines of CN 2-1 mainly in two groups, near 226.659543 GHz and 226.874764 GHz (Sutton et al. 1985). Thus, the line widths of CN 2-1 are broader than that of CS 5-4 in Arp 299 (see Figure 1), because of the confusion of CN 2-1 hyperfine lines. CN 2-1 is stronger than CS 5-4 in A and C regions (see Figure 1), while they are comparable in B region, with low signal to noise ratio (see Figure 1 and Table 1). A narrow CN 2-1 emission feature above  $5 \sigma$  with line width (FWHM) of less than  $100 \text{ km s}^{-1}$  was found in  $C'$  region, while no CS 5-4 emission was detected there (see Figure 2). With comparable CO emission in C and  $C'$  regions (Aalto et al. 1997; Casoli et al. 1999), the less CS 5-4 and CN 2-1 in  $C'$  than C region indicates that the dense gas fraction in  $C'$  is the lowest among the main gas components of A, B, C, and  $C'$  regions, in Arp 299.

The lack of HCN 1-0 (Aalto et al. 1997; Imanishi & Nakanishi 2006), CN 2-1 and CS 5-4 emission at B, C and  $C'$  regions with interferometer observations, indicates that there are weak extended emission of these dense gas tracers, because comparable emissions of dense gas tracers exist in B and C regions to that of region A based on the observational results with single dish telescope (Jiang et al. 2011). The HCN 1-0 flux in B, C and  $C'$  regions picked up by interferometer observation (Imanishi & Nakanishi 2006) was only about  $4 \text{ Jy km s}^{-1}$ , which was about 50% of that detected with single dish telescope (Jiang et al. 2011). With more sensitive interferometer observation (Casoli et al. 1999), almost all the HCN 1-0 flux was picked up. Further sensitive observations with millimeter interferometers or large single dish telescopes for lines with critical density higher than that of HCN 1-0, such as CN 2-1 and CS 5-4, are necessary to derive spatially resolved distribution of weak extended dense gas in Arp 299.

Dense gas fraction in different regions had been determined by line ratios of CO/HCN 1-0 (Casoli et al. 1999), which were  $7 \pm 1$  in A,  $20 \pm 1$  in B,  $45 \pm 8$  in C, and  $29 \pm 2$  in  $C'$  regions. So, if the critical density of HCN 1-0 is used as the threshold of dense gas, the dense gas fraction is the highest in A and lowest in C( $C'$ ), while in between in B regions. With several times lower critical density than that of HCN 1-0, HCO<sup>+</sup> 1-0 showed different properties than that of HCN 1-0 (Imanishi & Nakanishi 2006), with HCO<sup>+</sup>/HCN 1-0 ratio of 1.2 in A, 4.0 in B, and 2.1 in C regions. However, if the critical density of HCO<sup>+</sup> 1-0 is used as the threshold, A and B regions do have similar dense gas fraction with CO/HCO<sup>+</sup> 1-0 ratio of  $\sim 5.8$  in A and  $\sim 5.0$  in B, while C( $C'$ ) region with CO/HCO<sup>+</sup> 1-0 ratio of  $\sim 13.8$  to  $\sim 21.4$  has lower dense gas fraction than that of A and B regions.

The critical density of CN 2-1 is several times higher than that of HCN 1-0 and several times lower than that of CS 5-4 (Shirley 2015). Even though the CN 2-1 and CS 5-4 data are not sensitive enough to present high signal to noise ratio detections in B and C regions with velocity integrated map (see Figure 1), spectra in individual regions can still provide useful information to obtain line ratios of CS 5-4/CN 2-1 (see also Figure 1), just similar to what had been done for HCN/HCO<sup>+</sup> 1-0 in Imanishi & Nakanishi (2006). The velocity integrated intensities of CN 2-1 and CS 5-4 in A, B, and C regions are listed in Table 1. CS 5-4 was not detected in C region. Even though dense gas fraction in B region derived by HCN 1-0 to CO 1-0 ratio is about 1/3 of that in A region (Casoli et al. 1999), the line ratio

between CS 5-4 to CN 2-1 in B region is about 3 times of that in A region, which means the fraction of molecular gas with density higher than the critical density of CS 5-4 in B region is comparable to that in A region. On the other hand, with CN 2-1 emission and non-detection of CS 5-4 in C(C') regions, the fraction of molecular gas with density higher than the critical density of CS 5-4 in C(C') regions is lower than that of A and B regions. Dense gas fraction with different threshold traced by different dense gas tracers, including, HCO<sup>+</sup> 1-0, HCN 1-0, CN 2-1, and CS 5-4, provided slightly different properties in A, B, and C(C') regions. We suggest that the differences are mainly caused by volume density instead of astrochemical abundances of different tracers.

With generally consistent distribution of different dense gas tracers (HCN 1-0, CN 2-1, and CS 5-4) in Arp 299, the overlap starburst region (C and C') do have lower dense gas fraction than that of A and B regions supporting that starburst is stronger near the two nuclei than that of other regions. Similar results of higher dense gas fraction near two nuclei than other regions were also found for one early stage merger, the Antennae galaxy (Bemis & Wilson 2019). The efficient gas density increment near the nucleus due to the loss of angular momentum during merging process (Toomre & Toomre 1972) is more important than the overlap starburst activity, even though active overlap starburst can be found in some early and mid stage mergers. The overlap starburst may not be a common phenomenon during merging process of two gas-rich spirals, since there are many mergers without overlap starburst. For Arp 299, because the asymmetric molecular gas distribution in IC 694 revealed by CO lines (Aalto et al. 1997; Casoli et al. 1999), with the lack of molecular gas in the northeastern part of IC 694, the most possible way to form the overlap C and C' starburst regions was that NGC 3690 went across the northeastern part of IC694 during the merging process, which brings the gas from NGC 3690 and the northeastern part of IC 694 to C and C' starburst regions. Such process can explain the lack of molecular gas in the northeastern part of IC 694, much less molecular gas in NGC 3690 than that in IC 694, as well as the location of overlap starburst region, which is not in between the two galaxies (IC 694 and NGC 3690). The star formation activity traced by mid-IR emission at 38 $\mu$ m also presented similar properties to that of dense gas tracers in A, B, and C(C') regions, with 46% of the total flux density in A region, 22% in B region, 8% in C(C') in C region, and the remaining 24% as diffuse emission (Charmandaris et al. 2002). Thus, both the upcoming star formation traced by dense gas tracers and on-going star formation traced by infrared emission indicate that the activities of star formation rank from high to low as A, B, and C(C') regions.

#### 4. SUMMARY

With high resolution observations of CN 2-1 and CS 5-4 toward a mid-stage major merger Arp 299 with the SMA, we obtained spatial distribution of dense gas at about 3'' level. Most of CN 2-1 and CS 5-4 emissions are detected in the nuclear region of IC 694 (A), while only marginal detection of CN 2-1 and CS 5-4 are seen in NGC 3690 (B) and the overlap starburst region (C and C'). Highest CS 5-4 to CN 2-1 line ratio was found in B region among A, B and C regions of Arp 299. The dense gas fraction in different regions can vary with different threshold, observed with tracers with different critical densities, such as HCO<sup>+</sup> 1-0, HCN 1-0, CN 2-1, and CS 5-4. Dense gas fraction is the lowest in C(C') region, when dense gas tracers with critical densities higher than that of HCN 1-0, are used. The dense gas fraction decreases from A to B, C, and C' regions in Arp 299. The lack of CN 2-1 and CS 5-4 emissions in B and C+C' regions, together with strong emission of dense gas tracers there detected with single dish telescopes, implies there are weak extended emission of dense gas tracers in B and C+C' regions, which is similar to that of HCN 1-0 seen in Casoli et al. (1999).

Table 1. CN 2-1 and CS 5-4 velocity integrated intensities in A, B, and C regions.

Lines	A	B	C
CN 2-1	26.9 $\pm$ 1.0	3.9 $\pm$ 1.2	5.0 $\pm$ 1.4
CS 5-4	9.3 $\pm$ 0.9	4.3 $\pm$ 1.2	<3.3 (3 $\sigma$ )

Note: The velocity integrated intensities are based on the spectra shown in Figure 1, with the units of Jy km s<sup>-1</sup>.

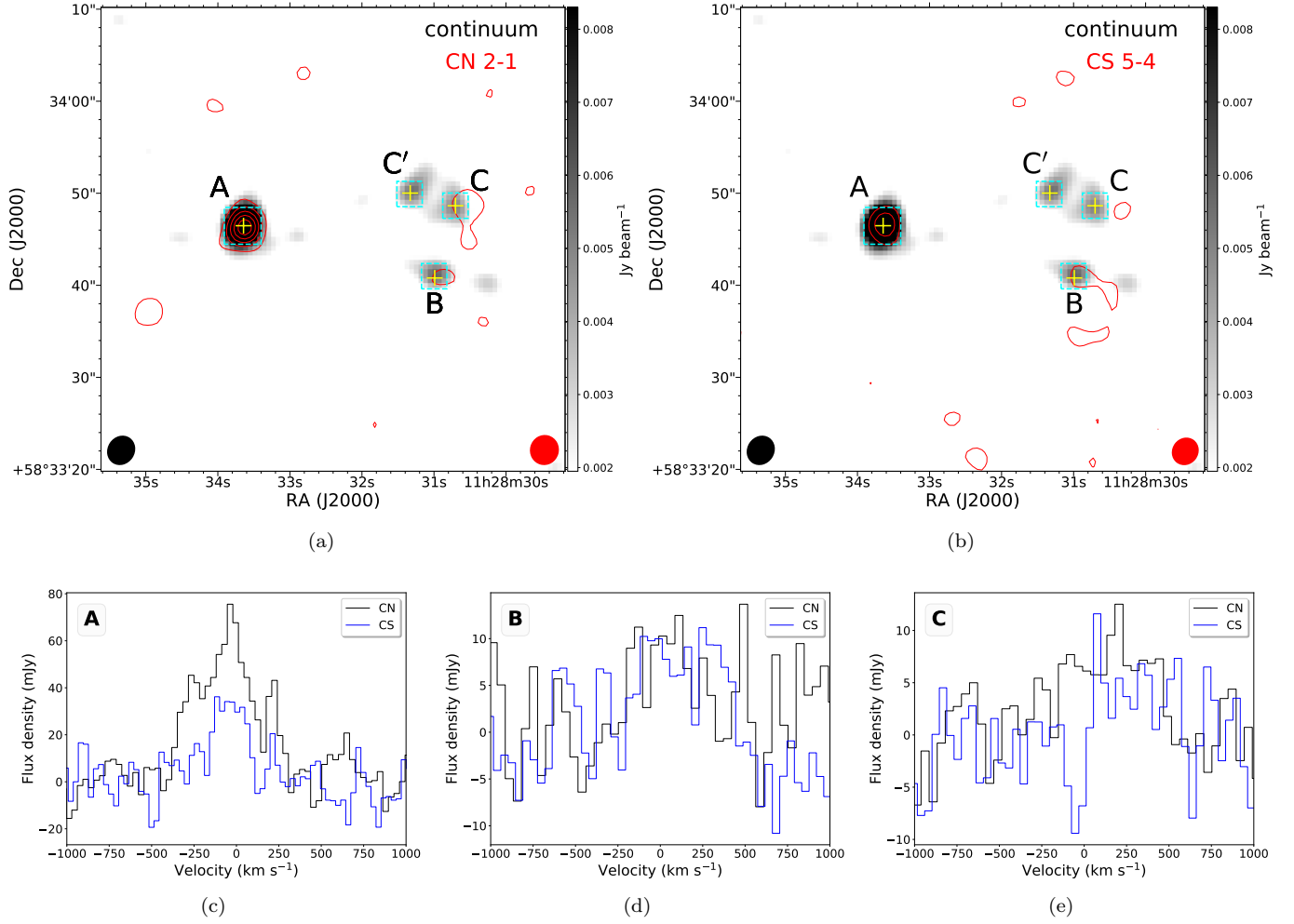


**Figure 1.** a. Spatial distribution of velocity integrated CN 2-1 (red contour) from  $-380$  to  $500$  km s<sup>-1</sup> overlaid on 1.3mm continuum (greyscale). The contour levels are 4, 8, 12, 16, 20,  $24\sigma$ , while  $1\sigma$  is  $1.33$  Jy km s<sup>-1</sup> beam<sup>-1</sup> and the beam is  $3.12'' \times 2.98''$  with  $P.A. = -15.25^\circ$  shown at the bottom right corner. The beam of 1.3mm continuum shown at the bottom left corner is  $3.14'' \times 2.79''$  with  $P.A. = -33.37^\circ$ , while  $1\sigma$  is  $6.5 \times 10^{-4}$  Jy. b. Velocity integrated CS 5-4 (red contour) from  $-180$  to  $500$  km s<sup>-1</sup> overlaid on 1.3mm continuum (greyscale). The contour levels are 3, 6,  $9\sigma$ , while  $1\sigma$  is  $1.22$  Jy km s<sup>-1</sup> beam<sup>-1</sup> and the beam is  $2.93'' \times 2.67''$  with  $P.A. = -36.95^\circ$  shown at the bottom right corner. c. Spectra of CS 5-4 and CN 2-1 within dashed box of region A. d. Spectra of CS 5-4 and CN 2-1 within dashed box of region B. e. Spectra of CS 5-4 and CN 2-1 within dashed box of region C.

We thank Prof. Yu Gao for helpful discussion. This work is supported by National Key Basic Research and Development Program of China (grant No. 2017YFA0402704) and the National Natural Science Foundation of China grant 12173067. We thank the anonymous referee for helpful comments, which improved the manuscript. The Submillimeter Array is a joint project between the Smithsonian Astrophysical Observatory and the Academia Sinica Institute of Astronomy and Astrophysics and is funded by the Smithsonian Institution and the Academia Sinica.

*Facilities:* SMA

*Software:* MIR, CASA

## REFERENCES

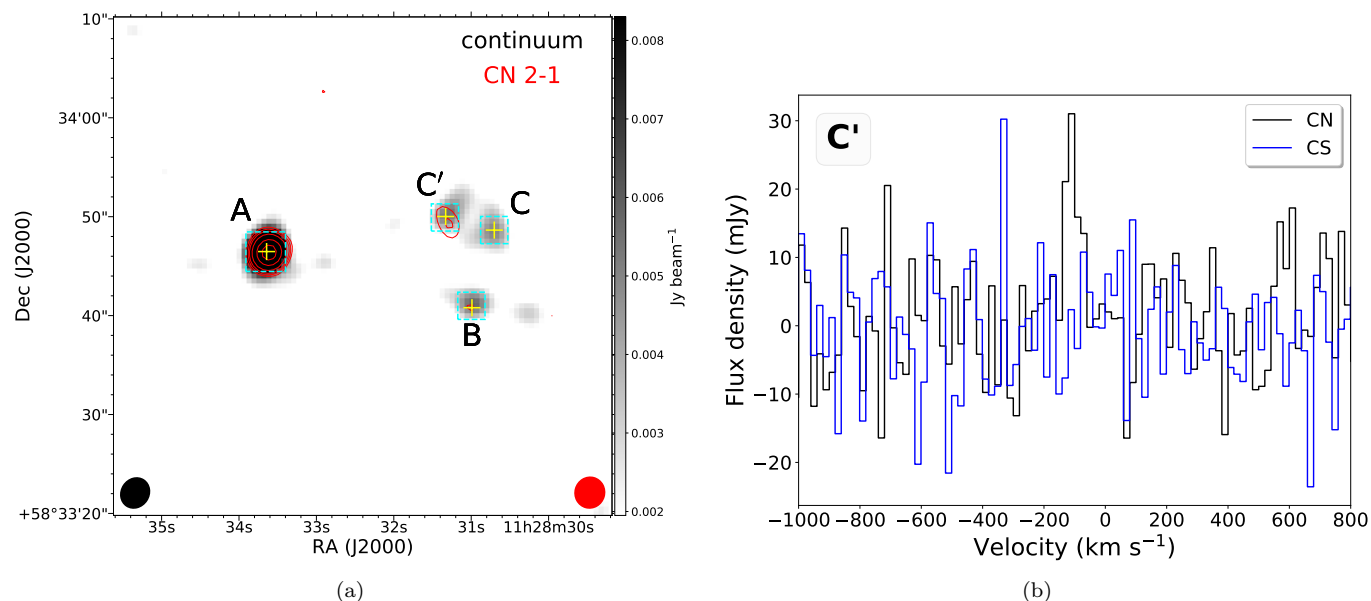


**Figure 2.** a. Velocity integrated CN 2-1 (red contour) from  $-180$  to  $-40$   $\text{km s}^{-1}$  overlaid on 1.3mm continuum (greyscale). The contour levels are 4, 5, 6, 8, 12, 16, 24  $\sigma$ , while  $1\sigma$  is  $0.53$   $\text{Jy km s}^{-1} \text{beam}^{-1}$ , with the same beam parameters described in Figure 1. b. Spectra of CS 5-4 and CN 2-1 within dashed box of region C'.

- Aalto, S. 2004, in *Astronomical Society of the Pacific Conference Series*, Vol. 320, *The Neutral ISM in Starburst Galaxies*, ed. S. Aalto, S. Huttemeister, & A. Pedlar, 3–14
- Aalto, S., Radford, S. J. E., Scoville, N. Z., & Sargent, A. I. 1997, *ApJL*, 475, L107, doi: [10.1086/310475](https://doi.org/10.1086/310475)
- Alonso-Herrero, A., Rieke, G. H., Colina, L., et al. 2009, *ApJ*, 697, 660, doi: [10.1088/0004-637X/697/1/660](https://doi.org/10.1088/0004-637X/697/1/660)
- Bemis, A., & Wilson, C. D. 2019, *AJ*, 157, 131, doi: [10.3847/1538-3881/ab041d](https://doi.org/10.3847/1538-3881/ab041d)
- Casoli, F., Willaime, M. C., Viallefond, F., & Gerin, M. 1999, *A&A*, 346, 663
- Charmandaris, V., Stacey, G. J., & Gull, G. 2002, *ApJ*, 571, 282, doi: [10.1086/339896](https://doi.org/10.1086/339896)
- Gao, Y., & Solomon, P. M. 2004, *ApJ*, 606, 271, doi: [10.1086/382999](https://doi.org/10.1086/382999)
- Harada, N., Sakamoto, K., Martín, S., et al. 2018, *ApJ*, 855, 49, doi: [10.3847/1538-4357/aaa70](https://doi.org/10.3847/1538-4357/aaa70)
- Ho, P. T. P., Moran, J. M., & Lo, K. Y. 2004, *ApJL*, 616, L1, doi: [10.1086/423245](https://doi.org/10.1086/423245)
- Imanishi, M., & Nakanishi, K. 2006, *PASJ*, 58, 813, doi: [10.1093/pasj/58.5.813](https://doi.org/10.1093/pasj/58.5.813)
- Imanishi, M., Nakanishi, K., & Izumi, T. 2019, *ApJS*, 241, 19, doi: [10.3847/1538-4365/ab05b9](https://doi.org/10.3847/1538-4365/ab05b9)
- Jiang, X., Wang, J., & Gu, Q. 2011, *MNRAS*, 418, 1753, doi: [10.1111/j.1365-2966.2011.19596.x](https://doi.org/10.1111/j.1365-2966.2011.19596.x)
- Lada, C. J., Forbrich, J., Lombardi, M., & Alves, J. F. 2012, *ApJ*, 745, 190, doi: [10.1088/0004-637X/745/2/190](https://doi.org/10.1088/0004-637X/745/2/190)
- Li, F., Wang, J., Gao, F., et al. 2021, *MNRAS*, 503, 4508, doi: [10.1093/mnras/stab745](https://doi.org/10.1093/mnras/stab745)
- Mao, R.-Q., Schulz, A., Henkel, C., et al. 2010, *ApJ*, 724, 1336, doi: [10.1088/0004-637X/724/2/1336](https://doi.org/10.1088/0004-637X/724/2/1336)
- Papadopoulos, P. P. 2007, *ApJ*, 656, 792, doi: [10.1086/510186](https://doi.org/10.1086/510186)
- Ramírez-Olivencia, N., Varenus, E., Pérez-Torres, M., et al. 2022, *A&A*, 658, A4, doi: [10.1051/0004-6361/202140822](https://doi.org/10.1051/0004-6361/202140822)
- Saito, T., Iono, D., Espada, D., et al. 2018, *ApJ*, 863, 129, doi: [10.3847/1538-4357/aad23b](https://doi.org/10.3847/1538-4357/aad23b)
- Sakamoto, K., Wang, J., Wiedner, M. C., et al. 2008, *ApJ*, 684, 957, doi: [10.1086/590484](https://doi.org/10.1086/590484)
- Scoville, N., Sheth, K., Walter, F., et al. 2015, *ApJ*, 800, 70, doi: [10.1088/0004-637X/800/1/70](https://doi.org/10.1088/0004-637X/800/1/70)
- Shirley, Y. L. 2015, *PASP*, 127, 299, doi: [10.1086/680342](https://doi.org/10.1086/680342)
- Sliwa, K., Wilson, C. D., Petitpas, G. R., et al. 2012, *ApJ*, 753, 46, doi: [10.1088/0004-637X/753/1/46](https://doi.org/10.1088/0004-637X/753/1/46)
- Solomon, P. M., Downes, D., & Radford, S. J. E. 1992, *ApJL*, 387, L55, doi: [10.1086/186304](https://doi.org/10.1086/186304)
- Springel, V., Di Matteo, T., & Hernquist, L. 2005, *MNRAS*, 361, 776, doi: [10.1111/j.1365-2966.2005.09238.x](https://doi.org/10.1111/j.1365-2966.2005.09238.x)
- Sutton, E. C., Blake, G. A., Masson, C. R., & Phillips, T. G. 1985, *ApJS*, 58, 341, doi: [10.1086/191045](https://doi.org/10.1086/191045)
- Toomre, A., & Toomre, J. 1972, *ApJ*, 178, 623, doi: [10.1086/151823](https://doi.org/10.1086/151823)

Wang, Z., Fazio, G. G., Ashby, M. L. N., et al. 2004, ApJS,  
154, 193, doi: [10.1086/423205](https://doi.org/10.1086/423205)

Yao, L., Seaquist, E. R., Kuno, N., & Dunne, L. 2003, ApJ,  
588, 771, doi: [10.1086/374333](https://doi.org/10.1086/374333)